Quantitative Calculation of Product Rovibrational Distributions from Atom−Diatom Exchange Reactions

Richard J. Marsh, Anthony J. McCaffery,* and Mark A. Osborne

Department of Chemistry, University of Sussex, Brighton BN19QJ, U.K.

Received: April 30, 2003

We describe a rapid, accurate method for calculating rovibrational distributions in diatomic products from elementary chemical reactions. The basis of the model is momentum interconversion at a critical configuration defined in terms of molecular dimensions of the species involved. This approach shares common elements with recent models of inelastic processes and the kinematic reactive model of Elsum and Gordon. We point out that these and related approaches represent a development of Newtonian mechanics equivalent to that followed in the conventional formulation of classical mechanics, but one in which motive force for change at the molecular level is attributed to dp/dt rather than to dV/dq. This leads to a particularly transparent form of mechanics that uses only familiar data such as bond length, mass, spectroscopic constants, and velocity, yet may be applied to the highly resolved single collision experiments of molecular reaction dynamics. We describe key aspects of the computational method, e.g., the definition of the critical configuration, the disposal of reaction enthalpy, the manner of assigning product vibrational states, and the way in which conservation of energy is ensured. Examples are chosen to illustrate the range of reactions to which the method may be applied. Each would represent a challenge to conventional theory. We show that velocity-angular momentum diagrams may be used to interpret data and to give physical insight into the origins of observed rotational distributions. Good agreement is obtained between experimental and calculated (v,j) distributions for a wide range of elementary reactions suggesting that our model, despite its simplicity, captures the principal physics of chemical change at the molecular level

1. Introduction

The mechanics of physical and chemical change has been a central topic of scientific investigation for more than 200 years,[1] and it remains an active field of study with rapid evolution of experiments that probe the elementary acts in greater and greater detail.[2] Despite the intensity of research we are still some distance from a clear, readily understood picture of the factors governing the outcome of reactive collisions at the microscopic level. Little has emerged that allows rule-of-thumb predictions or insight into causative relationships and few general principles that are transferable from one reaction to another. Progress in theoretical calculation is hampered by the complexity of the problem as conventionally formulated[3] and it is clear that only a massive increase in computational power will significantly increase the range of problems that may be tackled by this route. Nakamura[4] acknowledged the role played by development of computational technology in recent advances in quantum methods in molecular dynamics but concluded "*Much more effort should be spent on developing more illuminating approximate theories ... in order to elucidate the dynamics of larger systems*".

Is there a simpler approach that might be adopted, one that perhaps trades in some of the rigor of quantum scattering theory for insight and predictive power? If there is, it would be of wide-ranging benefit, but key criteria need to be met and critical questions answered. For example, in what way does any new approach differ from conventional methods and are there significant losses in the quest for greater transparency? What can we learn from experiment? How is any alternate form of mechanics operated? Finally, what are the advantages and the disadvantages of any new approach? Here we describe a model for chemical reactions that is strongly influenced by the methodology we have developed for treating nonreactive atom−molecule collisions.[5,6] This general method has proved remarkably successful in a wide range of inelastic processes, being both quantitative and revealing of causative relationships for effects observed.[7,8] Success in quantitative reproduction of a wide range of experimental data suggests that the method captures at least a substantial fraction of the physics of the collision event. Here we describe an extension of this model to the reactive domain placing detailed emphasis on how quantitative calculations may be performed. We also address the questions posed above as to how and in what regard the mechanics of collisions portrayed here differ from methods that are conventionally employed. As remarked in earlier publications[9] our approach has many elements in common with the so-called "kinematic, classical mechanical" model first proposed by Elsum and Gordon,[10] though we demonstrate that use of the term "classical mechanical" in this context is slightly misleading.

Detailed examination of the sophisticated experiments of molecular collision dynamics indicates that the physics controlling the outcome are considerably simpler than is conventionally portrayed. Of particular significance in this regard are the experiments of Hoffbauer et al.,[11] Parmenter and co-workers,[12] and McCaffery and Wilson.[13] The details of these and conclusions that may be drawn therefrom are discussed elsewhere.[7,8] It is difficult not to conclude from these data that provided quantization of molecular energy levels is appropriately recog-

10.1021/jp0305584 CCC: $25.00
Published on Web 10/22/2003

nized; they are best explained by the kinematics of momentum exchange between species having size and shape familiar to us from spectroscopy and diffraction. Furthermore, the motive force for change at the molecular level is most simply represented as momentum change (dp/dt), as first proposed by Newton, rather than as a variation of potential energy (V) with distance or angle (i.e., $\partial V/\partial q$) as in the later formulation of classical mechanics. As is well-known, classical mechanics was derived in the 19th century, substituting expressions for kinetic and potential energy into Newton's equations of motion to give the form now familiar to us as the Lagrangian or as Hamilton's equations.[14] This followed experiments on molecules in bulk phases, particularly gas ensembles by Clausius, Joule, and others, and led to the introduction of the concept of energy.[1] The experiments of modern molecular dynamics are considerably more detailed and varied than could be performed on macroscopic objects and constitute direct observation of single collision events rather than ensemble averages. When velocity and angle selection and detection are also added, these microscopic processes are found to be governed by simple Newtonian rules of momentum and angular momentum exchange within constraints set by quantization and by energy conservation.[13]

On reviewing a wide range of experimental evidence on the elementary collision event, we recently concluded[5] that momentum change provides the principal driving force for collision-induced events. This is seen clearly, e.g., in processes where energy change is small but angular momentum change is large or vice versa. The role of energy change appears to be to provide a quantum-state-specific threshold condition or constraint and an outer bound through overall energy conservation. The above attribution of the origin of motive force is implicit in the model devised by Bosanac[15] and by Beck et al.[16] to explain features of rotationally inelastic scattering. Their methods have been used very widely and with considerable success.[17] A quantitative model has been developed in which momentum and energy change are separable functions, and this reproduces a wide range of experimental data on nonreactive collisions.[6−8,18] In this angular momentum (AM) model, the probability of converting linear momentum of relative motion to angular momentum is calculated directly. By fitting extensive data sets, it was demonstrated[6] that this conversion occurs about a torque arm (b_n) whose maximum value is half bond length for a homonuclear diatomic (and the equivalent distance from the center-of-mass for a heteronuclear molecule). Gentry and co-workers[11] had earlier drawn the same conclusion from experiments on the Cl_2-Ar system. The physical principles of the AM model are transparent, and quantitative predictions can be made using only physical data on the system under study. Very clear indications of causative relationships are obtained from velocity (momentum)-rotational angular momentum plots.[7,8] Bosanac and co-workers[19] have reproduced the principal results of quantum mechanics using classical methods when coupled with the assumption of "Newton's fourth law", namely, that $P(x)\cdot P(p) = \hbar$ where $P(x)$ and $P(p)$ are classical probability densities of position and momentum. Our treatment contains somewhat similar assumptions though our approach follows Newton's second law more closely.

The application of these ideas to the reactive domain presents a number of difficulties. However, there appear to be grounds for believing[9] that the principles underlying the AM model may also apply in the case of chemical reactions and could form the basis of a quantitative model for atom−diatom exchange reactions. As previously remarked, our approach has much in common with that of Elsum and Gordon (EG)[10] in which orbital AM of relative motion of reactants is transformed into product species rotation on impact. Though not explicitly stated by the authors,[10] motive force for change in this method also is derived from momentum change. EG concluded their study with the remark, "*Presently the results of quasi-classical trajectory calculations are being over-interpreted in that explanations of product state distributions are sought in terms of features of the potential energy surface (PES) when in fact the principal features of the results can be explained without reference to the PES for the reaction.*" Here we describe a rapid, accurate method of calculating product vibrotational distributions in atom−diatom exchange reactions. In so doing, we give special emphasis to aspects that often are not fully described in simplified models; e.g., the definition of the critical configuration for reaction, the incorporation of reaction enthalpy, the assignment of product vibrational states, and the application of energy conservation. The method is applied to predict product vibrotational distributions from a number of chemical reactions that are sufficiently complex to represent a formidable challenge to current theoretical methods. Results are compared to experiment. We introduce a graphical representation similar to the velocity-AM diagrams of inelastic collisions[7,8] and use this to emphasize the point made by EG regarding the straightforward origins of features that are frequently attributed to complex excursions on the PES.

2. Calculating State-to-State Reaction Cross-Sections

Nuclear dynamical models of elementary chemical reactions are not new, though early approaches prior to the development of state-resolved product distributions were eclipsed by the successes of transition state theory.[20] The work of EG whose kinematic model is based on momentum interconversion in a highly localized spatial region has been mentioned above. Schechter and Levine[21] and others have demonstrated the effectiveness of this approach and extended it to a wide range of molecular contexts. The model that we describe shares many elements in common with that of EG, but it differs principally in the extent to which its formulation is informed by studies of inelastic collisions. Thus we endeavor to maintain a common set of physical principles for all molecular collision processes consisting of momentum conversion and exchange within constraints and boundaries set by energy conservation. No recourse is made to a computed PES, and the input data consists of only readily available physical information such as mass, bond length, and spectroscopic constants.

Reactive collisions are considerably more complex than are their inelastic counterparts. The most obvious complicating factor is the change in molecular identity that accompanies atom exchange and of origin of the coordinate frame about which orbital and rotational AM are defined. Problems arising from this change are dealt with through use of a mass-weighted coordinate system[22] as discussed extensively elsewhere[2,10] and not repeated here. A second, very evident difference is the enthalpy change that generally accompanies a chemical reaction. The manner in which reaction enthalpy is incorporated is discussed below. Other issues to be addressed within the model include the definition of the "critical configuration", the point at which momentum interconversion occurs, application of the energy conservation criterion, and how product vibrational state change is dealt with. These essential elements of a successful model, often not fully described when new approaches are presented, are discussed in more detail below.

2.1. Generation of Product Rotation. The assumption of instantaneous reaction within a localized spatial region permits

explicit expressions for product orbital and rotational AM to be written in terms of those of the reactants in the mass-weighted coordinate system. The derivation of these expressions was given by EG and in a more expanded form elsewhere.[2,21,23] We do no more than quote expressions relevant to this work. In the reaction A + BC → AB + C, the rotational AM (**j′**) generated within the product diatomic is given by[2]

$$\mathbf{j}' = \mathbf{l}\sin^2\beta + \mathbf{j}\cos^2\beta + \mathbf{d}\cos^2\beta \qquad (1)$$

Here, **l** is the orbital AM, and $\cos^2\beta$ is a mass weighting factor that relates dimensions in product coordinates to those of the reactants. Un-primed quantities refer to reactant's properties, and **d** is defined by

$$\mathbf{d} = ab\tan\beta[(\mathbf{R}_{A-BC}\times\dot{\mathbf{R}}_{BC}) + (\mathbf{R}_{BC}\times\dot{\mathbf{R}}_{A-BC})] \qquad (2)$$

In eq 2, *a* and *b* are square roots of reactant and product reduced masses, respectively.

The limiting cases of $\cos^2\beta \approx 0$ (heavy atom exchange) and $\cos^2\beta \approx 1$ (light atom exchange) are well-known.[2] In the former case, $\mathbf{j}' \approx \mathbf{l}$ where

$$\mathbf{l} = \mu_{A-BC}\mathbf{R}_{A-BC}\times\dot{\mathbf{R}}_{A-BC} \qquad (3)$$

and in the latter, when reactant **j** is small, then $\mathbf{j} \approx \mathbf{d}$. In practice contributions from both **l** and **d** must be evaluated. As mentioned above, our objective in formulating a model of reactive collisions is to retain as much commonality with inelastic collisions as practicable given the very obvious differences referred to earlier such as configuration and enthalpy change and, as we discuss in more detail below, method of assigning product vibrational state. Further aims are to avoid reference to a computed PES and, as far as possible, to keep the model parameter-free using only physical input data. This helps to develop a clearer picture of the physics governing the reactive process as well as greatly increasing the predictive power of the model.

2.2. The Critical Configuration. The existence of a critical configuration is a recurring theme in reaction rate theory and in simple models of reaction dynamics.[10,24] Related concepts are well-known in the field of inelastic collisions, for example the hard shape models of inelastic collisions representing the classical turning point at which momentum exchange occurs.[15] The point at which atom exchange occurs is more difficult to locate in reactive encounters, and different authors have defined this in different ways. Its significance in this context is that it constitutes the distance R_{A-BC} in eqs 2 and 3 about which the initial orbital AM is evaluated. EG use the ratio R_{BC}/R_{A-BC} to define the critical surface at which reaction occurs, and it takes the form of a sphere of constant radius differing with each reaction. Alternatively, it may be chosen to represent the peak of the barrier on the PES as suggested by Schechter, Levine, and Gordon.[21] Smith[24] has proposed a spherical critical coordinate modified by a line-of-centers threshold energy criterion.

In this work we wish to avoid recourse to a computed intermolecular potential and here explore the extent to which known physical quantities such as diatomic bond length may play a significant role in calculations and be used in the designation of the critical configuration. This is not only to maintain a link to our inelastic model where half bond length plays a key role as the anisotropy or maximum available torque arm[6] but also is part of efforts to find the simplest form of physics that will reproduce data with a reasonable degree of accuracy. Thus in Figure 1, if r_A is the distance from the center of the approaching atom (A) to the hard ellipsoidal surface of reactant homonuclear diatomic (BC), the critical configuration is defined by

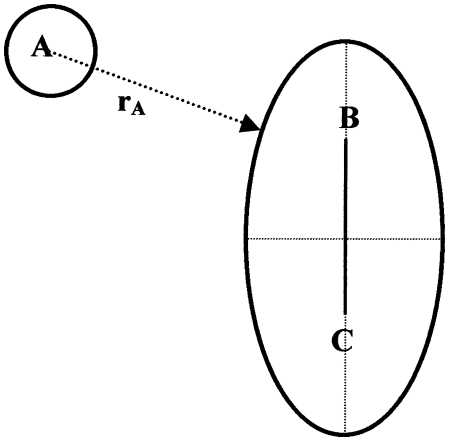

Figure 1. The critical configuration (defined by eqs 4, 5) is reached when atom A is in contact with the ellipsoidal surface representing the (homo-nuclear) reactant BC, i.e., when $r_A = R_A$.

$$r_A = R_{AB} - \frac{1}{2}R_{BC} \qquad (4)$$

R_{BC} and R_{AB} are equilibrium bond lengths of reactant and product diatomic, respectively. Using this definition, the critical surface is an ellipsoidal shape whose semimajor and semiminor axes are defined as

$$a^* = R_{AB} + \frac{1}{2}R_{BC} = 2R_B + R_A \qquad (5)$$

$$b^* = R_{AB} = R_A + R_B$$

R_{AB} and R_{BC} are product and reactant molecule equilibrium bond lengths, and R_A and R_B are the radii of atoms A and B. Note that the critical surface (for a homonuclear reactant diatomic) is then an ellipsoid of semimajor axis $= 2R_B + R_A$ and semiminor axis $R_B + R_A$. Thus, the shape representing the reactive surface is significantly larger than that at which momentum is exchanged in models of inelastic collisions, though the anisotropy is still half bond length (of the reactant diatomic). However, this no longer constitutes the maximum available torque arm.

2.3. Reaction Enthalpy. The reaction enthalpy is readily incorporated into theoretical models based on the PES such as quasi-classical trajectory or quantum mechanical calculations, but the expressions given above take no account of the energy release or intake that generally accompanies reaction. Methods such as the "direct interaction with product repulsion" (DIPR) model of Kuntz et al.,[25] particularly the "distributed as in photodissociation" (DIP) extension of Herschbach,[26] and the development of the DIPR-DIP to chemiluminescent reactions by Prisant et al.[27] all contain explicit prescriptions for energies absorbed and released, but the manner of dealing with reaction enthalpy is not always clearly expressed in kinematic models. Little experimental guidance is available on, e.g., the moment of energy release or on whether momentum is transferred between reactants before the change in configuration occurs. Both factors may have a significant effect on the outcome.

Here we make the commonly adopted assumption that no momentum exchange occurs prior to the nuclei reaching the critical configuration and that reaction occurs instantaneously at that point. Reaction enthalpy is dealt with by making the simplifying assumption we have previously introduced,[9] namely,

that the energy released (or absorbed) is converted into velocity of relative motion that is added to (or subtracted from) the initial relative velocity of the colliding species. The arguments for this are developed elsewhere,[9] but the principles are briefly stated. As the reactants approach, the relative velocity and angle of impact determine whether the outcome will be an inelastic encounter or a reactive one. As the nuclei slowly close in to the critical surface, the electrons of both species will have explored shared regions of space for (relatively speaking) some considerable time and if initial conditions (velocity, direction of approach) are suitable for forming a well-defined set of product molecule quantum states rather than simply a new set of reactant states then reaction ensues. The formation of AB constitutes the rapid development of an attractive force in an exothermic reaction representing the new AB bond, and this gives an additional impulse to the approaching nuclei in the direction in which they already are proceeding. This very simplistic approach is adopted here, and its ability to give acceptable answers for exothermic and endothermic reactions is tested on a number of elementary reactions for which rotationally resolved data have been reported.

2.4. Assigning the Product Vibrational State. Equations 1 and 2 define the rotational and orbital AM of the products in terms of reactant motion. However, they appear to suggest that product rotation alone will be observed as the outcome, yet we know from experiment that a number of product vibrational states may also be populated. The manner in which the product vibrational state is identified is not always well described in kinematic models, and it is not uncommon to report the total distribution of rotational states rather than to assign them to separate product vibrational states. The assignment of vibrational state in the model described here assumes, in common with others of similar type, that there is a Franck−Condon style transition from reactant to product state[10] with no change of position or momentum as this occurs. The formation of the new bond and the depletion of the old are so rapid that no momentum is imparted to the nuclei involved. With the definition of critical configuration as given above, the newly formed bond may be longer or shorter than the equilibrium bond length of the product diatomic depending on the position of the incoming atom on the critical surface. The stretch or compression in the new bond provides potential energy for the vibrational motion of the product diatomic. If this motion is assumed to be harmonic, the magnitude of the potential energy may be calculated from the molecule's force constant.

The kinetic energy associated with vibrational motion along the new bond is straightforwardly written since the product nuclear momenta are known, and thus the velocity component along the bond for each nucleus may be calculated from purely geometric considerations. The difference between these velocities separates internal (vibrational) motion from that of the center of mass, and the kinetic energy associated with product vibration is then readily calculated. The terms contributing to total vibrational energy in the product diatomic are

$$E_v = (1/2)k_{AB}(|r_{AB}| - R_{AB})^2 + (1/2)\mu_{AB}[(\dot{\mathbf{R}}_A - \dot{\mathbf{R}}_B).\hat{\mathbf{R}}_{AB}]^2 \quad (6)$$

The first term in eq 6 represents the potential energy of bond compression or stretch, k_{AB} is the force constant of the AB bond, and R_{AB} is the bond distance at the critical surface. The second term represents the kinetic energy of vibration, and $\hat{\mathbf{R}}_{AB}$ is a unit vector in the direction of the new bond. This expression assumes the vibrational motion to be harmonic and classical, which is reasonable for low degree of excitation in molecules having large vibrational energies. When this is not the case, a more realistic expression containing higher order terms may be used for the potential energy of nuclear displacement.

Calculations are carried out using the commonly used Monte Carlo averaging of initial conditions followed by binning of final states. In this latter step the vibrational quantum number of the product is the highest for which the energy is no greater than the total vibrational energy of the classically oscillating product as given by eq 6. The product rotational AM is binned in a similar manner, being defined by the highest total AM that does not exceed the value of j′ calculated from eq 1. Product rotational and vibrational quantum numbers (v_f,j_f) may be determined independently by solving the polynomials

$$(v_f + (1/2))\hbar\omega_{eAB} - (v_f + (1/2))^2\hbar\omega_e x_{eAB} = E_v \quad (7)$$

$$j_f(j_f + 1) = \{|\mathbf{j}|^2\}/\{\hbar^2\} \quad (8)$$

rounding down v_f, j_f to the nearest integer in each case. In eq 7, the first-order correction term $\omega_e x_e$ is included, though will not always be required. Similarly, higher-order corrections may be necessary in eq 8.

2.5. Applying Energy Conservation. The expressions given above give product rotational and vibrational distributions for an arbitrary initial trajectory, but two other features have not yet been considered and often appear to be neglected in models of this type. The first of these is the expectation that reaction probability will have some dependence on the *direction* of the collision trajectory. For example, with the critical surface as defined above, the degree of vibrational excitation will be highly dependent on the point of impact. The product rotational state will also depend on impact site and angle of trajectory through the parameters of eq 2. The second aspect not yet fully specified is the manner in which energy conservation is ensured. The energy of the assigned rovibrational state must be consistent with the energy available from relative velocity of collision, reaction enthalpy, and that used for product recoil. With critical configuration and product vibrational excitation as determined here, very high values of v_f may be obtained though in actuality only a few of these will be energetically accessible. Energy conservation needs to be enforced, though this is somewhat complicated by the fact that small amounts of energy can be lost count of in the process of quantum state binning.

These two issues, stereochemistry of approach and conservation of energy, may be dealt with simultaneously by assuming that conservation of energy is a boundary condition on the reaction probability. Thus, for each trajectory a decision on its acceptability is made at the point of collision. If the product rovibrational state that would be formed if the reaction were to occur is consistent with overall energy conservation, then the trajectory is judged to be a reactive one. If this condition is not met, the reaction does not proceed and the collision is adjudged inelastic. This procedure is difficult to express in an analytic form but readily lends itself to computational methods. It allows state-to-state integral cross-sections and hence total reaction cross-section to be evaluated and greatly increases the accuracy with which product state distributions are reproduced. Some leeway must be incorporated into the energy conservation condition and a variety of techniques might be envisaged to allow for small discrepancies. Here our criterion for acceptability of a reactive trajectory is simply that the system's total energy after the collision does not exceed that before reaction.

There is a striking similarity between the manner in which energy conservation is applied here and the form this require-

ment enters into the AM model of inelastic collisions.[5,6] This similarity is of course no coincidence, its origin lying in the separation of probability densities of AM and energy change in the rotational transfer function. The basis of this approach, proposed as a result of analysis of a wide range of experimental data, is that the probability of a collision-induced inelastic process is determined by the probability of generating the appropriate amount of rotational AM for those channels that are energetically open. Thus the motive force arises from momentum interconversion. In computational models of collision-induced rotational, rovibrational, and rovibronic state change, trajectories that lead to a specific final quantum state and also obey the energy conservation condition are counted as contributors to the inelastic process. Those that fail to meet the former criterion are considered as having been scattered elastically. This model is found to be a quantitative predictor of a very wide range of inelastic processes[7,8,18] using bond length, mass, spectroscopic constants, and velocity distribution as input data.

2.6. Monte Carlo Averaging over Initial Conditions. The Monte Carlo method of averaging single scattering events with initial conditions chosen at random weighted by their probability distributions is well-known, and little needs to be added here. The coordinate system coincides with the center-of-mass of the reactant, and all incoming reactant atom trajectories are parallel to the *y*-axis with an offset in the other two directions. The ellipsoidal critical configuration is initially aligned with the major axis along the *z*-axis and rotated in the *yz*-plane by a random angle θ. This is equivalent to the more usual method of using a single offset parameter and rotating the ellipsoid in two planes. The next step involves random selection of phase and magnitude of vibrational motion of the reactant that reflects the initial vibrational state energy. The semimajor ellipsoid axis is then modified to take account of the vibrational displacement. The trajectory is then followed and the point of impact (if any) calculated. If no impact occurs, then a new set of initial conditions is chosen and the process is repeated. The relative positions and momenta of the nuclei on impact are then calculated (including the vibrational momentum of the reactant molecule at the start of the trajectory) and used in eq 1 to determine the product rotational AM should a reaction have occurred. The vibrational energy of the product diatomic is also calculated from eq 6 and both vibration and rotation binned to the appropriate quantum states using the methods described above. The trajectory is then judged to be reactive or not, according to the energy conservation criterion described above; if this condition is met, the counter for that rovibrational product state is incremented by one and the process is repeated with a new set of initial conditions. The state-to-state cross-section is obtained from the relation

$$\sigma_{v',j'} = \pi b_{max}^2 \frac{N_{v',j'}}{N_T} \qquad (9)$$

Here, b_{max} is the maximum reactive impact parameter, $N_{v',j'}$ is the number of reactive trajectories leading to rovibrational state $|v', j'\rangle$, and N_T the total number of collisions.

3. Graphical Representation

An appealing feature of the AM model of *inelastic* processes is that the threshold conditions of rotational AM change and energy change may be represented in the form of velocity−(rotational) angular momentum plots.[5−8] These graphs are process-specific in a manner that permits qualitative prediction

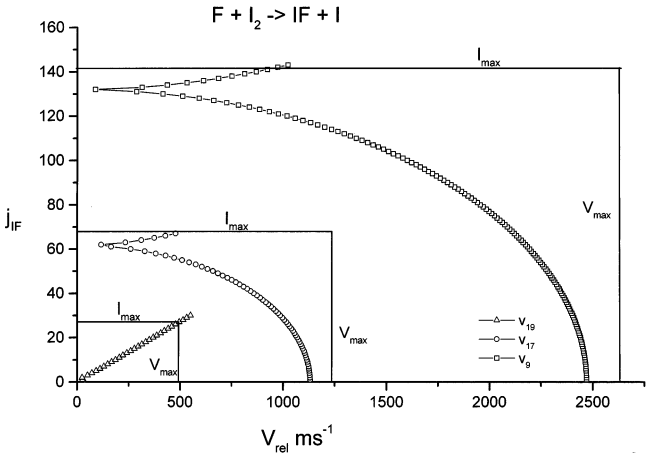

Figure 2. Velocity-AM plot for j_{IF} levels of $v = 9$, 17, and 19 in IF from the reaction F + I_2. See text of Section 3 for a full description.

of the principal features of vibrotational distributions in a wide range of inelastic processes. In this section, we demonstrate that related diagrams may be constructed for reactive collisions and that these may be used both to predict the principal features of product distributions and to infer the microscopic mechanisms that are responsible for them. In the inelastic case the velocity-AM plot graphs the channel-opening relative velocity (or momentum) for two processes. The first (the "*A*-plot") is the principal mechanism, linear-to-angular momentum conversion about a maximum torque-arm (b_n^{max}) set as half bond length (for a homonuclear diatomic) via the equation $\Delta j = \mu v_r b_n^{max}$. The second, (the "E-plot") is the state-to-state energy conservation criterion expressed in generic form as $1/2\mu v_r^2 = |\Delta E|$ where v_r is relative velocity, μ = reduced mass, and ΔE is the energy gap between initial and final states.

In the case of a chemical reaction, the product (v,j) states are those of the new species and final level spacings, and hence ΔE values, must reflect this change. In addition, the array of product energy levels must be placed on an energy scale the zero of which is set by initial reactant levels. Hence the product rovibrational states are displaced down or up the energy scale according to whether the reaction is exothermic or endothermic. As an illustrative example we choose the reaction F + $I_2 \rightarrow$ IF + I, one on which we have also performed quantitative calculations, as described in Section 4. This is an exothermic reaction and the difference between reactant and product dissociation energies $\Delta D_0 = -1.226$ eV. The zero of energy for calculating energy gap calculations (the *E*-plot) is taken to be that of the initial reactant state, assumed in this case to be non-rotating and in the lowest vibrational state, i.e., $(v_0,j_0)_{react}$ plus the effective collision energy (actual collision − recoil energy). This latter quantity is sometimes referred to as the translational exoergicity.[2]

The plots represent disposal of initial energy (collision energy plus reaction enthalpy) into rotation once a given vibrational channel has opened. There is an *E*-plot for each final vibrational level and the $j_{IF} = 0$ velocity is related to the energy needed to open that vibrational channel. As in the case of vibration−rotation transfer in inelastic processes,[18] vibrational energy is treated as a barrier that must be overcome before rotation within that level may be generated. Thus the energy available for rotation decreases as vibrational level increases. The principal features are seen in Figure 2 where *E*-plots for transitions to $v_{IF} = 9$, 17, 19 from the reaction F + $I_2 \rightarrow$ IF + I are displayed. The arched shape of the curves representing transitions to $v_{IF} = 9$, 17 reflects the diminishing energy gap as j_{IF} increases and

eventually becomes near resonant with the reactant energy zero. The range of j_{IF} values accessible for $v = 17$ is considerably less than that for $v = 9$ as the figure makes clear. The reaction liberates a pulse of energy the greater part of which, in this $\cos^2\beta \approx 0$ case, must be disposed into product rotation via the mechanism of orbital-to-rotational AM interconversion. This amount varies with the final vibrational state and sets an upper limit on the rotational channels that may be populated within a particular v_{IF} manifold.

The process by which reactant orbital AM is converted to product rotation at the critical configuration was discussed in Section 2. The reaction F + I_2 → IF + I has mass weighting factor $\cos^2\beta \approx 0$ and thus from eq 1, $j_{IF} \approx l_{A-BC}$. The maximum value of initial orbital AM (l_{max}) is readily calculated from eq 3. This will vary with final vibrational state, being largest for low product vibrational levels. Examples are shown in Figure 2 ($v = 9$, 17, 19) as the horizontal lines representing $l_{max} =$ 143 and 68 and 24 for $v = 9$, 17, and 19, respectively. The vertical lines show the maximum velocity available for conversion to orbital AM for that v_f state. Note that, in accordance with eq 1, all of the initial orbital AM must end up as product rotation with no recoil orbital AM and so access to the lower j_{IF} states of the $v = 9$, 17 manifolds cannot be through glancing collisions in which only a fraction of the initial velocity becomes the effective velocity. The l_{max} for a particular v_{IF} state is calculated for the case when R_{A-BC} is its maximum value. However, there will be many trajectories for which this maximum value is not reached and this will depend on the point of impact. Thus transitions to j_{IF} less than maximum value shown in Figure 3 will occur from trajectories for which $l < l_{max}$, i.e., torque arm values that are less than the maximum value obtainable at the critical configuration. The *E*-plots show channel opening conditions for all accessible rotational levels of $v = 9$, 17, 19, and it is clear that channels close to the maximum available will be especially favored for the first two of these levels. In a forthcoming publication,[28] we describe how the diagrammatic form presented in Figure 2 may be developed to yield quantitative vibration−rotation cross-sections. Here they are utilized for their ability to give a qualitative indication of the shape of final rotational distributions. Thus, for example, it is clear from Figure 2 that the overall rotational distribution shapes are likely to be similar for two of the cases displayed with principal peak at $j_{IF} = 133$ for $v = 9$ and $j_{IF} = 62$ for $v =$ 17. Both will have a "tail" of probabilities down to low j_{IF} values. The distribution is predicted to be very different in the case of $v = 19$. We discuss these qualitative predictions in more detail below and show that the energy level structure plotted in velocity-(rotational) AM space as in Figure 2 is an excellent predictor of the product vibrotational distribution.

4. Comparison with Experiment

In this section we examine how well the model predicts rovibrational distributions for a number of reactions, each of which has been the subject of detailed experimental investigation with full rotational resolution of product vibrational states. The examples were chosen to be widely varying in such factors as reaction enthalpy, atomic size and mass, and closeness to the so-called kinematic limit.[2,26] In each Monte Carlo calculation 2×10^6 random trajectories were followed, a number chosen to obtain a reasonably smooth final distribution. The process is computationally rapid, and input data consist of spectroscopic and other physical parameters that are readily available, none of which is adjusted. Calculations yield state-to-state absolute cross-sections, though these quantities are not always available from experiment, and consequently much comparison is on a relative scale. Where quantitative data are reported, comparisons are on an absolute basis.

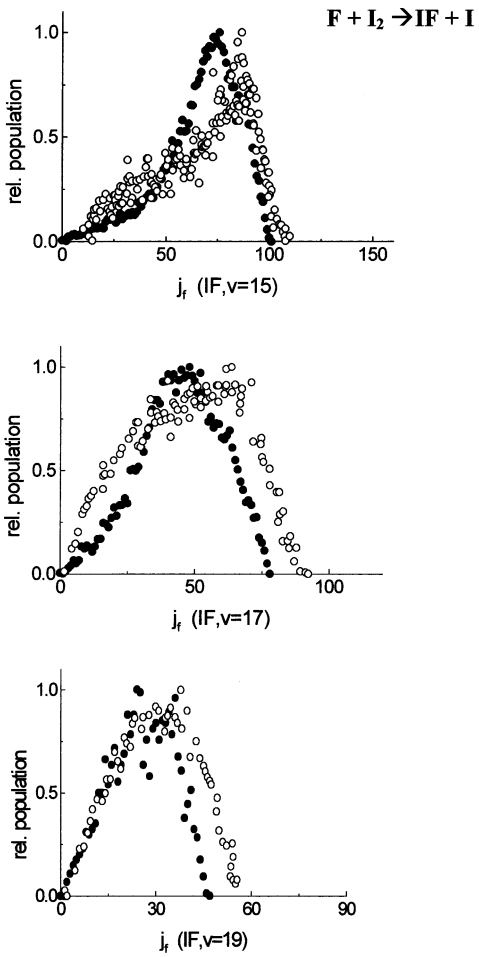

Figure 3. Experimental (open circles) and calculated (filled circles) rotational distributions in product IF molecules from the reaction F + I_2 → IF + I for final vibrational states $v_f = 15$, 17, 19. Experimental data from Girard et al.[18]

4.1. The Reaction F + I_2 → IF + I. The F + I_2 (v_i,j_i) → IF (v_f,j_f) + I reaction is of interest for a number of reasons. The use of a narrow line probe laser allowed Girard et al.[29,30] to resolve rotational distributions for the very large numbers of vibrational and rotational states of the product IF molecules emerging from this reaction and thus the reproduction of these constitutes a stringent test of any model. Furthermore, the rotational distribution in many of the v_f states is bimodal, a subject much discussed in the context of this[31] and other reactions.[32,33] Quasi-classical trajectory (QCT) methods have been employed to predict the outcome of this reaction[31,34] in which the number of open states makes a quantum mechanical (QM) calculation impractical. Girard et al.[29,30] resolved and identified around 10^4 vibrotational levels though data from states below $v_f = 8$ were not measurable due to strong pre-dissociation in the B-state of IF. Products having v_f levels up to 20 and others with j_f to 202 are reported and in such highly excited states anharmonicity and centrifugal distortion play a significant role.

Predicted product rotational distributions for $v_f = 15$, 17, 19 are shown in Figure 3 together with the experimental data of Girard et al.[29,30] In an earlier publication we compared calculated and experimental distributions for $v_f = 9-12$ and it is clear from these and the data presented in Figure 3 that the method reproduces experimental data with a high degree of accuracy.

The bimodal structure appears in all v_f states from $v = 9-17$ and that the rotational distribution is well reproduced in calculations over such a wide range of v_f,j_f states is very encouraging. Some discrepancies are found in the region of predissociation and at high v_f. In the latter case this reflects the sensitivity of the j_f distribution to the vibrational energy. Terms up to second order were included in the calculation, but in IF the series expansion converges only slowly. Not shown here are the results of calculations for $v_f = 0-8$ as there are no experimental data with which to make comparison. These distributions are found be narrow and centered on high j_f states, though evidence of bimodality persists.

Bimodal rotational distributions have been reported in other reactions, particularly those involving hetero-nuclear reactant diatomics,[32,33] e.g., H + ICl→ HCl + I; HCl + I → HI + Cl; and Ba +HI → BaI + H. An explanation put forward for bimodality in the first two of these relies on the suggestion that two groups of pathways exist on the potential energy surface, one of which generates high j_f through large impact parameter glancing collisions initially with the larger atom of the diatomic followed by migration to the smaller atom whereupon reaction ensues.[31] Low j_f in this interpretation results from direct collisions with the smaller atom of the reactant diatomic. In the case of Ba + HI, the bimodal distribution is attributed to competition between constraints arising from energy and from AM conservation.[33] It is difficult to sustain the two-pathway argument for a homonuclear reactant, particularly when a direct interaction model such as that described here reproduces the structure so closely. Competition between energy and AM constraints, as proposed by Kalogerakis and Zare,[33] however is a constant theme in the interpretation we present.

The origin of bimodality in IF distributions from F + I_2 becomes apparent on examining the velocity-AM diagrams shown in Figure 2. Constraints arise from the large energy gaps associated with transitions to low j_{IF} and these diminish as j_{IF} increases, reaching a minimum at $j_{IF} = 132$ for $v = 9$ and $j_{IF} = 61$ for $v = 17$ before rising again and run out of energy at $j_{IF} = 143$ and 68 for $v = 9$, 17, respectively. The velocity-AM diagrams predict a peak in the j_{IF} distribution at values for which the energy constraints are minimized and a broadened "tail" down to low j_{IF}. This latter feature will be elongated at low v and more compressed for high v values. These j_{IF}-dependent constraints arise entirely because of the energy level structure of the rovibrational states of IF and their juxtaposition in energy relative to that of the reactants in their initial condition. This interpretation is confirmed on inspection of the velocity-AM diagram for transitions to $v = 19$ in which the bimodal structure is found to be absent.[29,30] Figure 2 makes evident the substantial differences that are to be expected for $v = 19$. Vibrational levels 18 and 19 are accessed only through velocity of relative motion since they lie higher in energy than (v_0,j_0) of the reactants. The arched structure of the *E*-plot that is the dominant feature of transitions to all of $v = 0$ to $v = 17$ disappears for $v = 19$ to be replaced by a steadily climbing plot displaced from zero by a velocity related to the vibrational energy gap.[7,8,18] A single peak is predicted for transitions to $v = 19$, therefore. Figure 3 shows that these qualitative features of the j_{IF} distributions are quite accurate. In the $v = 19$ data, population of j_{IF} states beyond 25−30 is indicative of backscatter.

Figure 3 displays experimental and predicted j_{IF} distributions for $v = 15$, 17, 19, and in an earlier publication[9] we showed calculated and experimental data for $v = 9,10,11,12$. The results are in excellent agreement with experiment, and it is clear that this simple orbital-to-rotational AM exchange model using

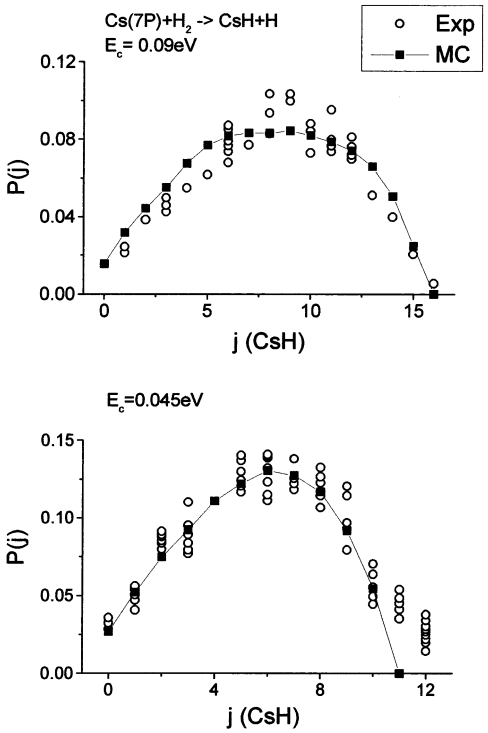

Figure 4. Experimental (circles) and calculated (squares) rotational distributions in CsH molecules ($v_f = 0$) from the reaction Cs(7P) + H_2 → CsH + H at collision energies 0.09 eV (upper panel) and 0.045 eV (lower panel). Experimental data from L'Hermite et al.[26]

readily available spectroscopic and kinematic data has captured the principal physics of this particular reaction. In terms of absolute cross-sections, reliable experimental data are hard to obtain because of the predissociation problem discussed earlier. We calculate the total cross-section for reaction to be 20 Å^2. This value may be compared to that of 72 ± 18 Å^2 reported by Appleman and Clyne[35] and 30 Å^2 calculated by Elofson and Holmlid.[36] In view of the uncertainties this can be regarded as a satisfactory level of agreement.

4.2. The Reaction Cs(7P) + H_2 → CsH + H_2. This reaction is very strongly endothermic when the reactants are in their ground states, and while such an energy deficit is often overcome by increasing the relative velocity of collision L'Hermite et al.[37] found the reaction to be feasible when the Cs atom is excited to a high-lying electronic state. This represents a significant challenge to a simple model such as that proposed here since it raises the question of how such excitation should included. Can electronic energy be incorporated in the same manner as reaction enthalpy as a modification to the relative velocity? In an attempt to answer this question we follow the approach outlined above but now with the Cs atom electronically excited and compare calculated product distributions for the reaction Cs(7P) + H_2 → CsH ($v_f = 0$) to experimental data.[37] This process raises the total energy of reactants just above that of products by an amount dependent on the Cs atom's spin−orbit state. Calculations here are reported for Cs in the $7P_{1/2}$ state at collision energies 0.045 and 0.09 eV. The enthalpy for the reaction Cs($7P_{1/2}$) + H_2 → CsH + H is 0.0016 eV.

Calculated *j*-distributions for CsH ($v = 0$) are shown in Figure 4 for $E_{coll} = 0.09$ and 0.045 eV together with experimental data.[37] As in the reaction discussed in the previous subsection, agreement between experiment and calculation again is very good. The lower collision energy data show small discrepancies at high j_f, though we note measurements in this region are

thought to be affected by the presence of para-H_2 in the reactant molecular beam.[37] The calculated total reaction cross-section at 0.09 eV is 5.0 Å^2 while that for the reaction at 0.045 eV is 1.1 Å^2. This latter value is in good agreement with experiment, L'Hermite et al.[37] reporting a value of 1 Å^2 for the lower energy reaction. Thus the incorporation of *electronic* excitation in the Cs atom in the form of the equivalent relative velocity, as adopted in dealing with reaction enthalpy, produces results that are in good quantitative agreement with experiment. L'Hermite et al.[37] have interpreted CsH product rotational and angular distributions in terms of a harpoon process that occurs at a neutral−ionic curve crossing in the entrance valley of the potential at around 7−8 Å and said to control the magnitude of the total reactive cross-section. This interpretation is supported by Gadea et al.[38] on the basis of their computed potential energy surface for this reaction and by the quantum calculations of Lepetit et al.[39] It is clear from the results of this study that a good match to experimental rotational distributions and overall reaction cross-section is obtained from the direct momentum exchange process at a critical configuration defined by molecular dimensions. Whether or not a harpoon mechanism is actually in operation can be neither proved nor disproved by the success of our calculation. We can, however, be clear that a quantitatively accurate account may be obtained without invoking long-range electron transfer.

4.3. The Reaction Al + O_2 → AlO + O. The oxidation of Al by O_2 is one of the few metal oxidation reactions that may be studied as a homogeneous process in the gas phase. In addition, the $(X)^2\Sigma^+ \rightarrow (B)^2\Sigma^+$ transition of AlO is conveniently located in the blue-green region for laser monitoring of product vibrotational distributions on formation. In the context of this study, the reaction constitutes a valuable test of the model because the process is only slightly endothermic and furthermore has no measurable activation energy.[40,41] As a result, it is possible to examine the conversion of velocity of relative motion into product rotation independently of effects due to the presence of a barrier or those depending on the timing of enthalpy release. Rotationally resolved experimental data for AlO $v = 0, 1$ are available on this system[41] from the pioneering metal oxidation studies under beam-gas conditions by Zare and co-workers. In their experimental study of Al + O_2, Dagdigian et al.[41] also determined the spread of relative velocities and these data are used in the calculation reported here. For each individual trajectory the initial relative velocity was chosen with probability proportional to the probability density for that value measured by Dagdigian et al. and thus our calculation represents the conditions of the experiment with reasonable accuracy.

Calculated and experimental results are shown in Figure 5 in the form of N_f distributions for $v_f = 0, 1$. The data are on a relative scale. The line-width of the laser employed in probing the $v = 1$ level precluded the measurement of low N_f populations for the $v = 1$ vibrational state. Dagdigian et al.[41] found that phase space theory did not give a good account of the AlO rotational distributions, unlike the BaO products from Ba + O_2 for which angular distributions[42] suggest the formation of a long-lived state. The authors concluded that the Al + O_2 reaction proceeds at least in part via a direct mechanism.[41] This would be accord with the findings reported here where Figure 5 indicates excellent agreement with experiment. The success of the nonreactive version of this model in predicting vibrotational distributions in inelastic collisions[7,8,18] indicates that the method employed here should be very reliable when the enthalpy contribution and the barrier are both low as in the case of this oxidation reaction.

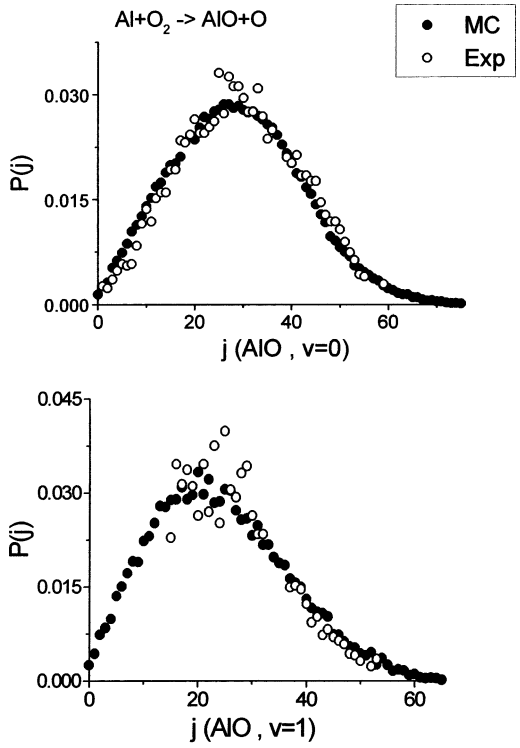

Figure 5. Experimental (open circles) and calculated (filled circles) rotational distributions in product AlO molecules from the reaction Al + O_2 → AlO + O for $v_f = 0, 1$. Experimental data from Dagdigian et al.[28]

4.4. The Reaction Ba + HI → BaI + H. The reactions discussed thus far have considered exchange between an atom and a homo-nuclear diatomic and for these the critical configuration is straightforwardly defined in terms of reactant and product diatomic bond lengths through the ellipsoid representation. This approach may also be satisfactory for a hetero-nuclear reactant, provided the sizes of the two atoms are not too dissimilar, though the offset center-of-mass must be taken into account. If the atomic size difference is large then a new definition of the critical configuration will generally be needed. Such an example is HI where the shape is more akin to that of an egg with the H-atom appearing as a small bump on the nearly spherical surface that is the I-atom. To represent a hetero-nuclear molecule, the symmetry of the ellipsoid shape along the bond axis is reduced by introducing a new (z^3) term into the standard ellipsoid formula to give

$$\frac{z^2}{a^2} + \frac{z^3}{c^3} + \frac{x^2 + y^2}{b^2} = 1 \qquad (10)$$

The parameter c has units of length and its magnitude is related to the degree of asymmetry of the hetero-nuclear species and will vary from molecule to molecule. The point of intersection of this surface and an incoming trajectory will have three roots, and a limiting (minimum) value of c may be identified for which all three roots are real for all values of $x^2 + y^2 \leq b^2$. This is the egg-shape limit where the large atom end of the molecule is spherical and since in these circumstances the parameter c is related to a and b, the model remains free of adjustable parameters. Away from this limit a decision must be made on the magnitude of c on the basis of, for example, the atomic sizes or alternatively this distance could be parametrized.

Very detailed experimental and theoretical studies have been carried out on the Ba + HI → BaI + H reaction by Zare and

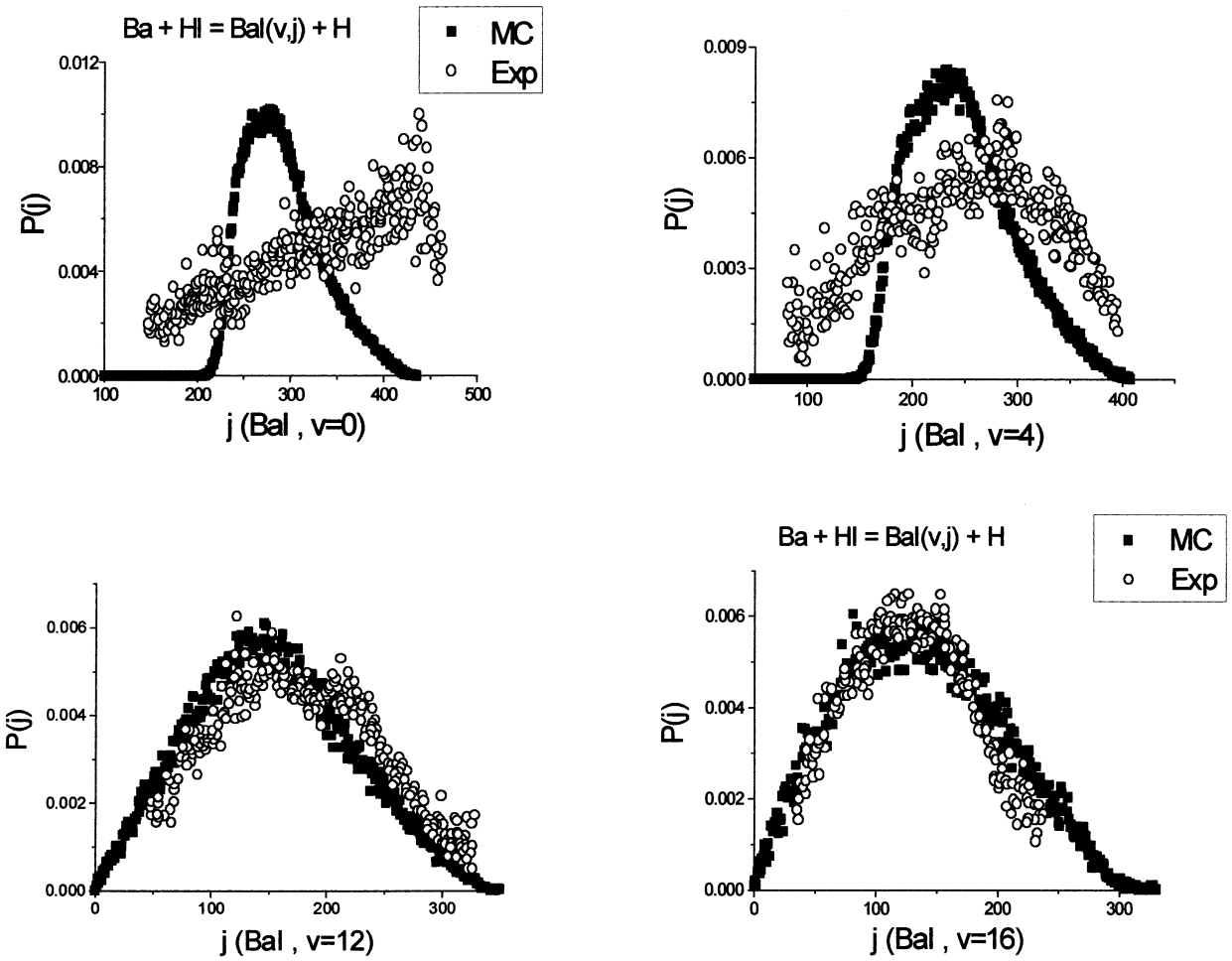

Figure 6. Experimental (open circles) and calculated (filled squares) rotational distributions in product BaI molecules from Ba + I_2 → BaI + I for $v_f = 0$, 4, 12, 16. Experimental data from Tsekouris et al.[29]

co-workers,[33,43,44] and here we compare calculated vibrational and rotational distributions to those obtained in beam-gas experiments by Tsekouris et al.[43] These authors report rotational distributions for $v_f = 0$, 4, 8, 12, 16, 18. More precise data are available from the crossed beam experiment of Kalogerakis and Zare though the range of v_f that could be studied was much reduced compared to the beam-gas experiment. The Ba + HI system has aroused considerable theoretical interest in view of the closeness of the reactant and product masses to the so-called kinematic limit[2,26] of $\beta \approx 90°$ in which all orbital AM of relative motion may in principle be converted to product rotation.

The experimental distribution of relative velocities[43] was incorporated into the calculation in the form of a triangular function with most probable v_{rel} at 590 ms^{-1} and minimum and maximum values at 125 and 1125 ms^{-1}, respectively. Predicted (v_f,j_f) distributions are displayed in Figure 6 together with experimental data.[43] From these it is clear that for the lowest v_f states the accuracy is not very good, with that for $v_f = 0$ being particularly poor. The reported distributions at low v_f, particularly that for $v_f = 0$, look quite similar to what might be expected from a phase space theory calculation[45] and the existence of a long-lived state for accessing the $v_f = 0$ channel would not be totally unexpected. The amount of energy that must be deposited into internal motion is very large indeed, populating very high BaI rotational states. The generation of appropriate amounts of recoil orbital angular momentum in this system is much constrained by the low reduced mass of the departing fragments, however, and this is perhaps the reason for the unusual shape of the low v_f rotational distributions. However this interpretation is somewhat contradicted by the results of the crossed beam study of this system. In this experiment the $v_f = 0$ rotational distributions reported by Kalogerakis and Zare[33] for several different collision energies are narrow and are reproduced very accurately indeed by our calculations.

The product (v_f,j_f) distributions are found to be a strongly varying function of E_{coll} at low collision energies,[43] and structure suggestive of bimodal behavior appears in the crossed beam experiment as E_{coll} is lowered.[33] The authors attribute this to competition between the role of the centrifugal barrier and of energy conservation in determining the maximum impact parameter and hence the reaction cross-section, the former dominating at low energy and the latter at high. In terms of our model, the likelihood of long-lived state formation in low product vibrational states is expected to rise when the enthalpy contribution to reaction energy exceeds that contributed by collision energy and this would be exacerbated by low reduced mass of product fragments. A similar situation arises in the vibrational pre-dissociation of van der Waals trimers as we have recently demonstrated.[46] A large pulse of energy must be disposed into rotation (for the $v_f = 0$ case) within a framework of overall angular momentum conservation. This is likely to become more difficult as the orbital AM of initial relative motion is reduced. Thus the unusual distribution of j_{BaI} states in $v = 0$ from the beam-gas experiment may signify long-lived state formation for the low velocity end of the distribution that is absent in the higher velocity crossed beam case. This bimodality is not reproduced in our calculations though it would not be difficult to integrate the statistical elements of phase space theory

into our model in a calibrated fashion. We note that agreement between calculated distributions and experiment for the higher v_f levels is very encouraging. For these, the energy "load" that must be disposed into rotation has been reduced by exciting vibrational motion. Since v_f levels up to 30 are populated in this reaction, the overall picture is likely to be quite positive if experiments could be extended to encompass the full v_f distribution.

4.5. Other Reactions. In an earlier publication[9] we compared results of calculations with experiment and with quantum mechanical calculations for the reactions $H + D_2 \rightarrow HD + D$ and $Cl + H_2 \rightarrow HCl + H$. In both of these reactions agreement was good. Less satisfactory is the predicted (v_f,N_f) distribution in OH from the reaction $H + O_2 \rightarrow OH + O$ at $E_{coll} = 1.6$ eV. In this highly endothermic system, agreement with the experimental rotational distribution for $v_f = 0$ reported by Bronikowski et al.[47] is good, but that for $v_f = 1$ is less satisfactory. Distribution shapes are close to experimental, but the latter extend to higher j_f than predicted and this is quite marked for $v = 1$. The experimental data in the latter case has some resemblance to a phase space theory distribution,[45] and although the kinematics of this reaction are very different from those of the Ba + HI case discussed above there are significant similarities in terms of available orbital angular momentum and a rationalization of the observations in the terms described above may be possible. The product vibrational branching ratio agrees well with experiment, but absolute cross-section is somewhat higher than that reported.[48]

5. Summary and Conclusions

The model described here represents a significant improvement in terms of accuracy and generality in the nuclear dynamical approach to calculating outcomes of reactive collisions. This is achieved using insights obtained from the AM model of inelastic processes[5−8] while retaining the critical concepts introduced by EG[10] to the field of reactive collisions. In this work we have added explicit detail regarding (i) definition of the critical configuration at which momentum interconversion occurs in terms of reactant and product bond lengths, (ii) incorporation of reaction enthalpy, (iii) assignment of v_f states, and (iv) manner in which energy is conserved. The result is a computationally rapid, parameter-free technique that predicts product vibration−rotation distributions with an accuracy that belies the simplicity of the physical principles and the ready availability of input data. The spatial region in which reaction occurs is defined in terms of a 3-D hard shape, the critical configuration, of size determined by reactant and product bond lengths with no reference to the PES.

In the model the motive force driving physical or chemical change at the microscopic level is momentum change with energy conservation acting as a constraint within which the mechanism operates, an approach adopted following analysis of data from highly resolved collision dynamics experiments.[5,13] It should perhaps be emphasized that the development of methods of *rotational* state resolution in molecular dynamics has proved critical in this respect. The result is a very economical form of mechanics that has the virtue of transparency and treats molecules as real physical objects while recognizing the existence of quantization of molecular levels. This relates very directly to the postulates of Newton with later discoveries, such as the concept of energy and quantization, incorporated in the manner that retains Newton's original identification of the source of motive force. The fact that molecular shape and size, energy level separation, and other well-established experimental observables are the key parameters in this and the related model for inelastic collisions is very valuable in terms of visualization of the process and may be of more fundamental significance.

The dimensions of the critical configuration play an important role in defining initial orbital and hence final rotational AM and also in the identification of product vibrational state. Product vibrational level is assigned according to the sum of two terms, one the kinetic energy arising from the momenta of the nuclei of the product in the direction of the newly formed bond, the other a potential term arising from the displacement of the new bond from its equilibrium distance. The latter term is primarily governed by point of impact on the critical configuration. In the reaction $F + I_2 \rightarrow IF + I$ where around 20 v_f states are populated, accurate assignment of vibrational levels is crucial to obtaining meaningful j_f distributions in each manifold. It is evident from Figure 3 that the method is both effective and reliable. Peaks and bimodal structures of the rotational distributions are reproduced, as are trends in degree of bimodality as the vibrational ladder is climbed. We have introduced a reactive analogue of the velocity-angular momentum diagram and demonstrate its use in gaining additional physical insight into the origins of the principal features of the vibrotational distributions. The $F + I_2$ reaction constitutes a stringent test of any model and the predicted v_f,j_f distributions are sufficiently close to experiment to indicate that the principal physics of the process are captured in the model.

Good agreement with experiment is obtained for reactions that are exothermic, those that are endothermic, and for $Cs + H_2 \rightarrow CsH + H$, a reaction that proceeds only when the Cs atom is highly electronically excited. Results on hetero-nuclear species suggests that further work might need to be done to define a robust critical configuration for these reactant molecules though it should be stressed that the overall picture in predicting v_f,j_f distributions in $Ba + HI \rightarrow BaI + H$ away from the low v_f case in beam-gas data is very encouraging. Discrepancies between experiment and calculated distributions in two cases discussed here may provide evidence of long-lived intermediate states. There are some similarities in these two examples, and plausible kinematic arguments may be constructed to account for this behavior. This may permit some degree of predictive power and may have wider application.

Finally we return to the remarks of Elsum and Gordon[10] who cautioned against automatic recourse to details of the intermolecular potential in seeking to explain features of product rovibronic distributions. The apparent bimodality in j_{IF} from the $F + I_2$ reaction constitutes a cautionary tale. An important message contained in this and related publications[5−8,18] is that the application of a small number of fundamental principles involving energy and angular momentum can give a great deal of insight into collision-induced processes both reactive and nonreactive. The calculations described here are very rapid and the data needed to perform them is readily available. The use of diagrammatic methods gives considerable insight into the processes at work when molecules collide, an aspect that will be amplified in a forthcoming publication.[28] However, Figure 2 and the discussion of Section 3 make clear that an appropriately scaled energy level diagram for reactants and products is a very useful starting point for analyzing data from fully resolved collision dynamics experiments, and this becomes a very powerful tool when energy and AM variables are plotted in velocity-angular momentum space.

Acknowledgment. M.A.O. thanks the Royal Society for a University Research Fellowship.

References and Notes

(1) Mason, S. F. *A History of the Sciences*; Macmillan: New York, 1962.

(2) Levine, R. D.; Bernstein, R. B. *Molecular Reaction Dynamics and Chemical Reactivity*; Oxford University Press: Oxford, U.K.; 1987.

(3) See, for example, *Discuss. Faraday Soc*. **1998**, *110*. *Chemical Reaction Theory*.

(4) Nakamura, H. *Annu. Rev. Phys. Chem*. **1997**, *48*, 299.

(5) McCaffery, A. J.; AlWahabi, Z. T.; Osborne, M. A.; Williams, C. J. *J. Chem. Phys.* **1993**, *98*, 4586.

(6) Osborne, M. A.; McCaffery, A. J. *J. Chem. Phys*. **1994**, *101*, 5604.

(7) McCaffery, A. J.; Marsh, R. J. *J. Phys. B* **2001**, *34*, R131.

(8) McCaffery, A. J.; Marsh, R. J. *Phys. Chem. Commun*. **2001**, *4*, 112.

(9) Truhins, K.; Marsh, R. J.; McCaffery, A. J.; Whiteley, *J. Chem. Phys.* **2000**, *112*, 5281; McCaffery, A. J.; Truhins, K.; Whiteley, T. W. J. *J. Phys. B* **1998**, *31*, 2023.

(10) Elsum, I. R.; Gordon, R. G. *J. Chem. Phys.* **1982**, *76*, 3009.

(11) Hoffbauer, M. A.; Burdenski, S.; Giese, C. F.; Gentry, W. R. *J. Chem. Phys*. **1983**, *78*, 3832.

(12) Clegg, S. M.; Burrill, A. B.; Parmenter, C. S. *J. Phys. Chem. A* **1998**, *102*, 8477; Parmenter, C. S.; Clegg, S. M.; Krajnovich, D. J. *Proc. Natl. Acad. Sci*. **1997**, *94*, 8387.

(13) McCaffery, A. J.; Wilson, R. J. *Phys. Rev. Lett.* **1996**, *77*, 48; McCaffery, A. J.; Wilson, R. J. *J. Phys. B* **1997**, *30*, 5773.

(14) See, for example, Pauling L.; Wilson E. B. *Introduction to Quantum Mechanics*; McGraw-Hill: New York, 1935; Chapter 1.

(15) Bosanac, S. *Phys. Rev. A* **1980**, *22*, 2617.

(16) Beck, D.; Ross, U.; Schepper, W. *Z. Physica A* **1979**, *293*, 107.

(17) Kreutz, T. J.; Flynn, G. W. *J. Chem. Phys*. **1991**, *93*, 452; Serri, J. A.; Bilotta, R. M.; Pritchard, D. E. *J. Chem. Phys*. **1982**, *77*, 2940; Marks, A. J. *J. Chem. Soc. Faraday Trans*. **1994**, *90*, 2857.

(18) Marsh, R. J.; McCaffery A. J. *J. Phys. B* **2003**, *36*, 1363.

(19) Skenderovic, H.; Bosanac, S. D. *J. Mol. Struct. (THEOCHEM)* **1995**, *341*, 41.

(20) Eyring, H. *J. Chem. Phys*. **1935**, *3*, 107; Evans, M. G.; Polanyi, M. *Trans. Faraday Soc*. **1935**, *31*, 875.

(21) Schechter, I.; Prisant, M. G.; Levine, R. D. *J. Phys. Chem*. **1987**, *91*, 5472; Schechter, I.; Levine, R. D.; Gordon, R. G. *J. Phys. Chem*. **1991**, *95*, 8201; Schechter I.; Levine, R. D. *J. Chem. Soc., Faraday Trans*. **1989**, *85*, 1059.

(22) Eyring, H.; Polanyi, M. *Z. Phys. Chem. Abt. B* **1931**, *12*, 279.

(23) Smith, F. T. *J. Chem. Phys*. **1959**, *31*, 1352.

(24) Smith, I. W. M. *J. Chem. Educ*. **1982**, *59*, 9.

(25) Kuntz, P. J.; Mok, M. H.; Polanyi, J. C. *J. Chem. Phys.* **1969**, *50*, 4623.

(26) Herschbach, D. R. *Faraday Discuss. Chem. Soc.* **1973**, *55*, 244.

(27) Prisant, M. G.; Rettner, C. T.; Zare, R. N. *J. Chem. Phys.* **1984**, *81*, 2699.

(28) McCaffery, A. J.; Osborne, M. A.; Marsh, R. J. In preparation.

(29) Girard, B.; Billy, N.; Gouédard G.; Vigué J. *J. Chem. Phys.* **1988**, *88*, 2342; Girard, B.; Billy, N.; Gouédard, G.; Vigué, J. *Faraday Discuss. Chem. Soc*. **1987**, *84*, 65.

(30) Girard, B.; Billy, N.; Gouédard, G.; Vigué J. *J. Chem. Phys*. **1991**, *95*, 4056.

(31) Firth, N. C.; Keane, N. W.; Smith, D. J.; Grice, R. *Faraday Discuss. Chem. Soc.* **1987**, *84*, 53; Fletcher, I. W.; Whitehead, J. C. *J. Chem. Soc. Faraday Trans. II* **1982**, *78*, 1165.

(32) Lagana, A.; Gervasi, O.; Crocchianti, S.; Garcia, E.; Deaspuru, G. O.; Alvarino, J. M. *Can. J. Chem*. **1994**, *72*, 919; Breckenridge, W. H.; Umemoto, H. *J. Chem. Phys*. **1981**, *75*, 4153.

(33) Kalogerakis, K. S.; Zare, R. N. *J. Chem. Phys.* **1996** *104*, 7947.

(34) Fletcher, I. W.; Whitehead, J. C. *J. Chem. Soc. Faraday Trans. 2* **1984**, *80*, 985; Keane, N. W.; Whitehead, J. C.; Grice, R. *J. Chem. Soc. Faraday Trans. 2* **1989**, *85*, 1081.

(35) Appelman, E. H.; Clyne, M. A. A. *J. Chem. Soc. Faraday Trans. 1* **1975**, *71*, 2072.

(36) Elofson, P.; Holmlid, L. *Chem. Phys*. **1994**, *178*, 315.

(37) L'Hermite, J. M.; Rahmat, G.; Vetter, R. *J. Chem. Phys.* **1990**, *93*, 434.

(38) Gadea, F. X.; Spiegelmann, F.; Pelissier, M.; Malrieu, J. P. *J. Chem. Phys*. **1986**, *84* 4872.

(39) Lepetit, B.; Le Dorneuf, M.; Launay, J. M.; Gadea, F. X. *Chem. Phys. Lett*. **1987**, *135*, 377.

(40) Fontijn, A.; Felder, W.; Houghton, J. J. *Chem. Phys. Lett.* **1974**, *27*, 365.

(41) Dagdigian, P. J.; Cruse, H. W.; Zare, R. N. *J. Chem. Phys*. **1975**, *62*, 1824.

(42) Dagdigian, P. J.; Cruse, H. W.; Schultz, A.; Zare, R. N. *J. Chem. Phys.* **1974**, *61*, 4450

(43) Tsekouras, A. A.; Leach, C. A.; Kalogerakis, K. S.; Zare, R. N. *J. Chem. Phys.* **1992**, *97*, 7220.

(44) Zhao, D.; Zare, R. N. *J. Chem. Phys.* **1992**, *97*, 6208; Noda, C.; McKillop, J. S.; Johnson, M. A.; Waldeck, J. R.; Zare, R. N. *J. Chem. Phys.* **1986**, *85*, 856.

(45) Pechukas, P.; Light, J. C.; Rankin, C. *J. Chem. Phys*. **1966**, *44*, 794.

(46) McCaffery, A. J.; Marsh, R. J. *J. Chem. Phys*. **2002**, *117*, 6478.

(47) Bronikowski, M. J.; Zhang, R.; Rakestraw, D. J.; Zare, R. N. *Chem. Phys. Lett*. **1989**, *156*, 7.

(48) Marsh, R. J.; McCaffery, A. J. Unpublished results.